

**GT2011-45483**

## **Design Optimisation of Casing Grooves using the Zipper Layer Meshing Method**

**Greg Carnie, Yibin Wang and Ning Qin\***,

Department of Mechanical Engineering, University of Sheffield, Mappin Street, Sheffield, S1 3JD, South Yorkshire, Great Britain

and

**Shahrokh Shahpar**

CFD Methods, Design System Engineering, Rolls Royce plc. Derby, DE24 8BJ, Derbyshire, Great Britain

*\*corresponding author: n.qin@sheffield.ac.uk*

### **ABSTRACT**

In an earlier paper by the authors [1], a buffer layer method for linking two non-matching structured meshes was introduced for computational simulation of multi-component geometries, each requiring high quality structured meshes. Based on the work, a new algorithm, named the zipper layer method [2], has been developed to link multi-block meshes for gas turbine applications. Numerical results for a turbomachinery rotor flow case are included to demonstrate the solution behaviour across the zipper layer. In the present paper, we will report our work on the optimisation of the casing groove geometries in relation to stall margin and efficiency of a transonic rotor using this new meshing methodology. Six grooves are parameterised by their independent depths and a width to gap ratio. An advanced response surface method based on Sobol Design of Experiment (DoE) and Krigging Response Surface Model (RSM) are used for the optimisation. A leave-one-out cross-validation (LOOCV) method is used to calculate the quality of the response surface metric. The final optimized groove configuration was obtained through an optimisation cycle using the Rolls-Royce SOPHY (SOFT-PADRAM-HYDRA) software [3], which not only improves the Stall Margin (SM) of the rotor but also maintains its peak efficiency. The optimized grooves on the casing side show large variations in their depth from upstream to downstream of the rotor.

### **1.0 INTRODUCTION**

In rotor design, a tip clearance is necessary, usually larger than aerodynamically desirable. The tip clearance is made as small as possible to account for the change in blade position at different operating conditions and for manufacturing limitations/tolerance. Two features of tip clearance flow are (1) the blockage, a fluid dynamic aspect and (2) the loss of efficiency which is a thermodynamic effect. The effects of casing treatments have been studied since the 1970's and one of the first documented examples is Osborn *et al.* [4] who looked at various casing treatments ranging from honey comb casings to circumferentially grooved casings. They found that the circumferentially grooved casing gave overall better performance in terms of maintaining efficiency and stall margin improvement. It has been well documented that tip clearance effects can reduce the operating range, pressure ratio and efficiency of a transonic axial compressor. Losses in the form of flow separation, stall and reduced rotor work efficiency are resulted from the tip leakage vortex (TLV) generated by the interaction of the main flow and the tip leakage jet induced by the blade tip pressure difference. Thus if one can weaken the effect that the TLV has on the main flow (i.e. improve the flow condition) the operating range of the compressor is expected to increase. The effects are more detrimental in transonic compressor due to the interaction of the shock with the TLV.

Suder and Celestina [5] showed that the interaction of the shock and the tip leakage vortex creates a large region of low-speed flow immediately downstream. The blockage leads to a high incidence angle at the blade tip at which point the rotor starts to stall. The region of low-energy fluid grows and moves closer towards the leading edge of the blade as the mass flow rate decreases. Adamczyk *et al.* [6] concluded that an injection of high energy flow in the forward part of the casing end-wall region could reduce the growth of the low-energy flow and thus increase the flow range of the rotor. If one can improve upon the tip region blockage, theoretically the pressure ratio, efficiency and mass flow can be increased. Casing treatment such as a stepped tip gap or “grooves” can alleviate the blockage and extend the operating range of the rotor. Thompson *et al.* [7] showed this using stepped casing treatment on a first stage transonic rotor. These stepped tip gap or “grooves” can increase the stable flow range of the compressor. The groove placement is very much dependent on the rotor configuration and speed as the blockage will occur at different regions around the blade for differing configurations. Shabbir and Adamczyk [8] showed that for a low speed rotor the groove casing should start near 10% chord of the rotor blade.

Therefore understanding the flow physics of the particular rotor under investigation is critical. By examining the flow region one can infer a good starting point for any optimisation or parametric study of any given rotor. Ito *et al.* [9] performed a parametric study of different circumferentially endwall configurations on Rotor 37. These endwall configurations improved the stall margin of the rotor when placed above the leading edge of the blade up to a position of around 10% axial chord. A parametric study casing treatment for Rotor 37 was carried out by Beheshti *et al.* [10]. A regular H-block mesh was used to complete the casing, onto which the casing treatment was made. This therefore required interpolation between the casing block and the rotor mesh below. They concluded that the endwall casing treatments control the TLV better at a tip gap size of 1.5% span.

More recently work carried out by Huang *et al.* [11] performed a parametric study of groove casing treatment for NASA Rotor 37. In their paper they showed two different groove configurations, both extended the operating range of the rotor. An overset grid was used to connect the groove mesh to the rotor mesh [12]. Interestingly their configurations had the placement of the first groove at 10% axial chord. Work by Choi *et al.* [13] performed optimisation of groove casing treatment also for Rotor 37. Their process used a radial basis neural network method. The grooves in this case were also not directly connected to the main mesh; instead they relied on a general grid interface method from ANSYS-CFX 11.0. Their numerical results seem to consistently under predict that of the experimental data. In their optimised configuration the first groove was placed right opposite to the rotor LE. However both papers [11,13] concluded that the

presence of the groove near the trailing edge was redundant. This was revealed when plotting the static pressure distribution near the blade tip.

In all the work reviewed here regarding the addition of groove casing treatment a grid interface is required with the fluxes being interpolated through the interface. The meshes used in this study have used a new mesh connection method, the zipper layer method [2], derived from the buffer layer method [1] which is much improved in accuracy and efficiency from its predecessor in connecting multi-block structured meshes, thus negating the requirement to interpolate the CFD and/or Navier Stokes fluxes.

This study aims to extend the operation range while maintaining the efficiency of an axial compressor, using the NASA Rotor 37 case as the test bed, through the introduction of casing treatment grooves. This is to be achieved by way of automated optimisation cycle process using SOPHY [3], Rolls-Royce’s in-house software and a novel technique, the zipper layer method that links multi-block meshes of different topologies. A design of experiment (DoE) method is used to generate the groove parameters utilising an LPtau sequence. LPtau is a quasi-random generator and the points belong to Sobol sequences are uniformly distributed in the N-dimensional unit cube [14]. A response surface model (RSM) will then be constructed and trained using Kriging [15] and a leave-one-out cross-validation method is used to verify the accuracy of the RSM. The optimum parameters are then determined by searching the RSM using simulated annealing (S.A.) optimization algorithm.

## NOMENCLATURE

ARMOGA	Adaptive range multi objective genetic algorithm
CFD	Computational fluid dynamics
DoE	Design of Experiment
LE	Leading edge
MB	Multi-block
PADRAM	Parametric design and rapid meshing
RMSE	Root mean square error
RSM	Response surface model
S.A.	Simulated annealing
SA	Spalart-Allmaras turbulence model
SOFT	Smart optimisation for turbomachinery
SOPHY	SOFT-PADRAM-HYDRA
TE	Trailing edge
TLV	Tip leakage vortex

## 2.0 TEST CASE

The NASA Rotor 37 test case is an isolated axial-flow compressor rotor designed and studied experimentally at NASA's Lewis Research Center (now NASA Glenn). The experimental mass flow rate required to achieve choked flow was determined to be  $\dot{m}_{choke} = 20.93\text{kg/s}$ . Two experimental data sets were taken at near stall and peak efficiency, with  $\dot{m}/\dot{m}_{choke} = 0.925$ , and at  $\dot{m}/\dot{m}_{choke} = 0.98$ , respectively.

The geometry of the blade can be found in the ARGARD report [16], details of which can be seen in Fig. 1. The rotor with boundary conditions can be seen in Fig. 2.

Rotor inlet hub-to-tip diameter ratio	0.7
Rotor blade aspect ratio	1.19
Rotor tip relative inlet Mach number	1.48
Rotor hub relative inlet Mach number	1.13
Rotor tip solidity	1.29
Rotor total pressure ratio	2.106
Rotor polytropic efficiency	0.889
Number of rotor blades	36
Equivalent rotor tip speed (m/s)	454.1
Equivalent rotational speed (rad/s)	1800
Nominal tip clearance (mm)	0.356 (0.45% span)

**Fig. 1** Blade geometry details extracted from AGARD report [16]

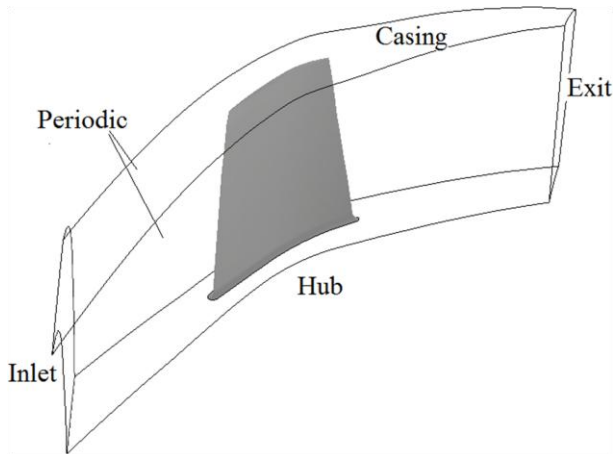


**Fig. 2** Outline of NASA Rotor 37 mesh generated in PADRAM with 2.5mm radius fillet at root of blade

The pressure ratio and adiabatic efficiency were calculated as follows:

$$PR = \frac{P_{outlet}}{P_{inlet}} \quad (1)$$

$$TR = \frac{T_{outlet}}{T_{inlet}} \quad (2)$$

$$\eta = \frac{\left( PR^{\frac{\gamma-1}{\gamma}} - 1 \right)}{TR - 1} \quad (3)$$

To be consistent with the AGARD report all the data present here are mass averaged.

## 3.0 NUMERICAL METHODS

A novel zipper layer grid generation method [2] has been implemented in the Rolls Royce grid generation and design suite PADRAM [17]. The purpose is to link a multi-block structured H-O type mesh around the rotor to a differently structured H-type casing mesh and compare both the numerical results regarding accuracy and efficiency to that when the O-H mesh is extended to the casing surface. Flow solutions have been carried out using the hybrid grids with/without the zipper layer, using the Rolls Royce flow solver Hydra [18]. Both sets of numerical results are compared and validate against the experimental results.

### 3.1 Zipper layer meshing method

The meshing technique used in this paper is a new and novel way to link multi-block structured meshes of different topologies. It functions like a “zipper” to bring together two multi-block (MB) meshes. This generic algorithm has in this instance been used to fully connect and link the MB mesh of the blade side mesh to that of groove mesh which has replaced the original casing block.

This new and novel approach adopts the same philosophy of the buffer layer mesh method [1] which generates a structured dominated grid by linking topologically different MB structured together via an unstructured buffer layer. The zipper layer method splits the structured cells at the interface to “zip” the MB structured meshes without overlapped cells. Different from the buffer layer mesh method, zipper layer mesh method uses an interface mesh to link the MB meshes on both sides, as shown in Fig. 3. Based on the interface mesh, a new node is introduced into the geometrical centre of each cell which needs splitting to form new cells. The similar cell splitting method as used in buffer layer method was adopted. The distinction is that in buffer layer method, points are only introduced into each zone; while in zipper layer method, points are introduced into each split cell. The zipper layer mesh method comprises the following steps:

- (a) Forming an interface by superimposing surfaces of two adjacent blocks, Fig. 3a;

- (b) Generating an unstructured interface mesh formed of triangles and quadrilaterals including all the mesh points from both surfaces and the intersection points, Fig. 3b;

Inserting nodes in the resulting hexahedra which need splitting; and joining the nodes to the unstructured interface mesh, so that an unstructured double layer of cells is produced at the interface between the blocks, comprising tetrahedra and pyramids, possibly with some hexahedra, Fig. 3c. Fig. 4 and 8 shows a practical demonstration of the zipper layer algorithm on NASA Rotor 37. In order for the interface mesh to be constructed one needs to determine which cell each of the surface nodes of the original meshes belong to. To achieve this a dual fast march method which is developed from fast march method [19] is applied to quickly locate the nodes. The dual fast march method search is quicker than a brute-force search as it only searches the local nearby cells. The original fast-march method algorithm was designed to search a single mesh only, whereas now the dual fast march method algorithm searches two meshes. For further details please consult [2].

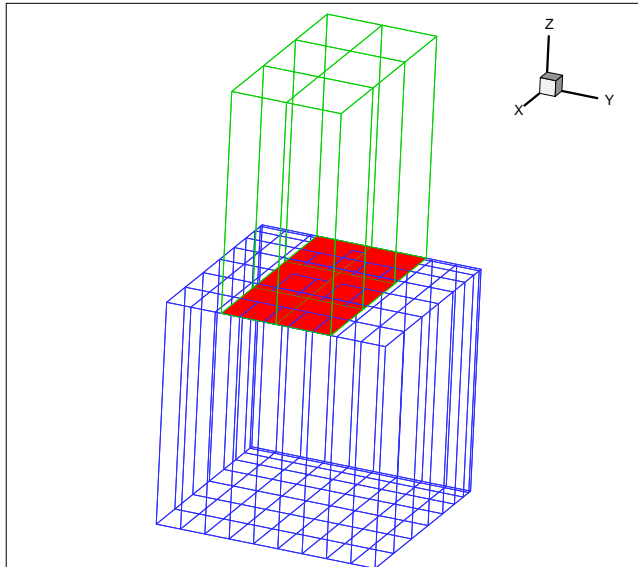


**Fig. 3a** Interface of two different structured meshes

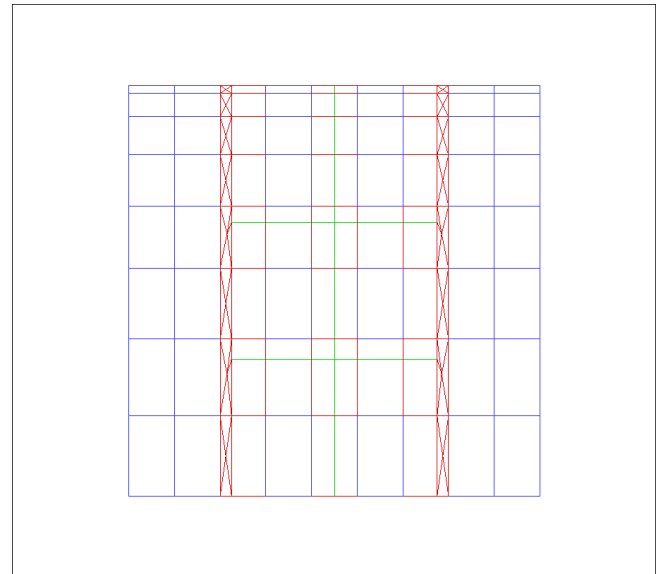


**Fig. 3b** Interface mesh (blue quads indicate the hexahedral remaining unchanged in the third step; while the rest of the quads form pyramids)

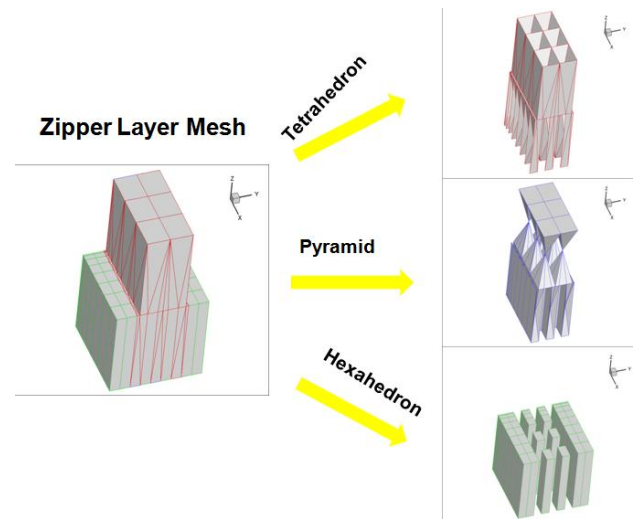


**Fig. 3c** Zipper layer mesh and the resulting elements

### 3.2 Validation of Zipper Layer Mesh for Rotor 37

Initial tests were performed to assess the feasibility of using the zipper layer mesh without casing treatment. The zipper layer links two structured meshes; the original multiblock mesh generated in PADRAM can be seen in Fig. 4. Fig. 5 shows the original multiblock mesh and a new structured mesh linked via a zipper layer for a clean annulus. The new H-block on the casing side of the zipper layer mesh will give a better base from which groove casing treatment can be added. The zipper layer will therefore allow for a fully connected mesh without the need for interpolation.

The Original structured multi-block mesh consists of five-H mesh blocks and one-O mesh block for the blade. The upstream H-block is 40x59x84, the downstream H-block is 50x59x84, both the passage H-blocks are 74x16x84, the H-block mesh above the blade tip is 86x17x16 and finally the O-mesh block representing the blade is 203x12x84. The resulting mesh when all blocks are merged gives a mesh consisting of 810,228 hexahedral elements. The zipper layer effectively splits a hexahedral layer either side of the interface mesh in the tip gap with unstructured cells, thus the total number of elements for this mesh increases to 1,070,609.

Each mesh shown in Fig. 4 and Fig 5. was run from choke to numerical stall and compared to the experimental data. Hydra was run as a steady state calculation with a 4 level multi-grid approach and a CFL=2.0. A wall function was employed and the SA turbulence model was used, all the solid walls were treated as non-slip adiabatic. A subsonic inflow condition was specified at the inlet where the total pressure and temperature profiles were set according to the data from the AGARD report [16]. A radial equilibrium subsonic boundary was used at the exit, this allows for a single pressure to be specified at a given radial point from which the exit pressure is calculated. By increasing the back pressure one will eventually reach numerical stall, just before this occurs at a given back pressure the mass flow has to have converged to a stable value and the flow residual and SA variable be converged to at least 6 orders.

As can be seen in Fig. 6 the zipper layer mesh compares well to both the experimental data [16] and that of the structured MB mesh for the total pressure. When comparing the computational efficiency to the experimental efficiency data it can be seen that for both mesh types they consistently under predict the result. It can therefore be concluded that the zipper layer result are as accurate as the structured mesh results. In the authors experience with various CFD codes that although the absolute values may differ significantly, the deltas (due to major design changes) are valid i.e. the delta holds across a range of CFD methods. This remarkable fact means that CFD does not have to predict the figure of merits in absolute terms accurately, but being able to “rank” accurately is the key for both design by analysis and automatic design optimisation. This therefore gives confidence when next grooves casing treatment is added to the zipper layer mesh. When normalised, the experimental near stall point is 0.925, whereas the structured MB mesh and the structured mesh MB with zipper layer is 0.910 and 0.907 respectively. The near stall mass flow rate for both meshes is therefore less than the experimental value by around 2%. However, to put this into perspective and highlight how sensitive the stall condition is computationally, a change in back pressure of only 0.6% (less than 900Pa) in the exit condition for the CFD calculation can give a normalised flow rate of either 0.925 or 0.910. Hence one needs to ensure that convergence is obtained correctly for

each mesh ran. To this end a change in back pressure of 100Pa is used to determine if a solution has indeed stalled.

The flow convergence history for the both meshes at their respective stall condition is shown in Fig. 7, both of which achieved full numerical convergence. The near stall condition is a very complex point to solve, and with the zipper mesh having more elements it was expected that at stall condition the zipper layer mesh would require more iterations. Each mesh was ran on 8cores using two 2.33Ghz E5410 Intel Xeon processors. The zipper layer had twenty five percent more elements than that for the structured MB mesh and this was reflected in the computational time. The total CPU time for the structured MB mesh was 8 hrs 47 mins and 16hrs 55mins for the zipper layer mesh. Although the mesh count is about 25% more, the convergence is also slower, making the total computational time to double for the most demanding case at stall. The comparisons at other conditions indicate that the total computational time is of similar order. For example at peak condition the CPU time are as follows: zipper layer mesh 4hrs 8mins 29secs; structured MB mesh 3hrs 47mins 56secs.

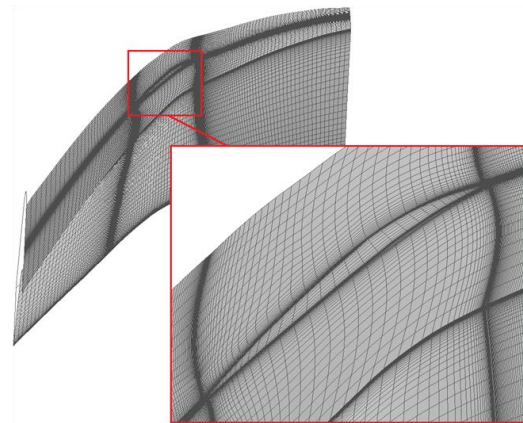


**Fig. 4** Original structured multiblock mesh

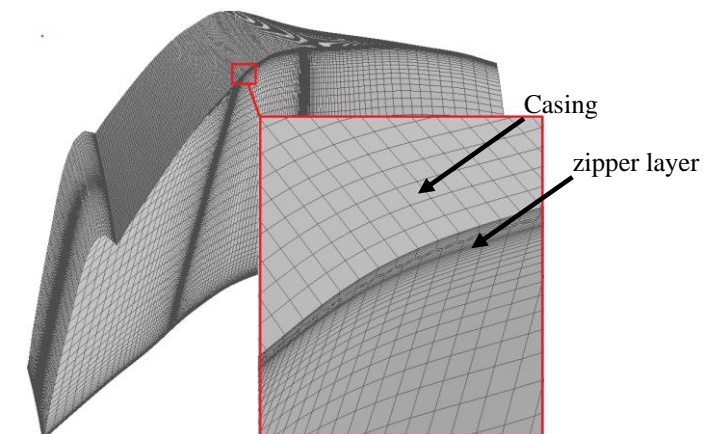


**Fig. 5** Mesh in Fig. 4 with zipper layer and new Generated in PADRAM casing side mesh

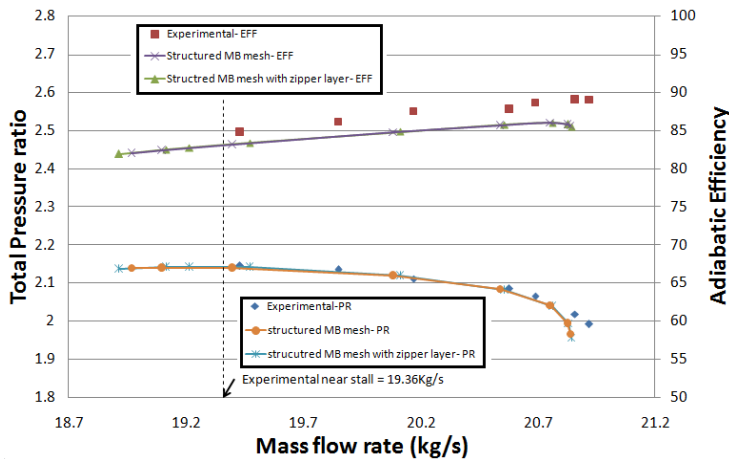


**Fig. 6** Numerical versus experimental data for validation of Rotor 37 flow

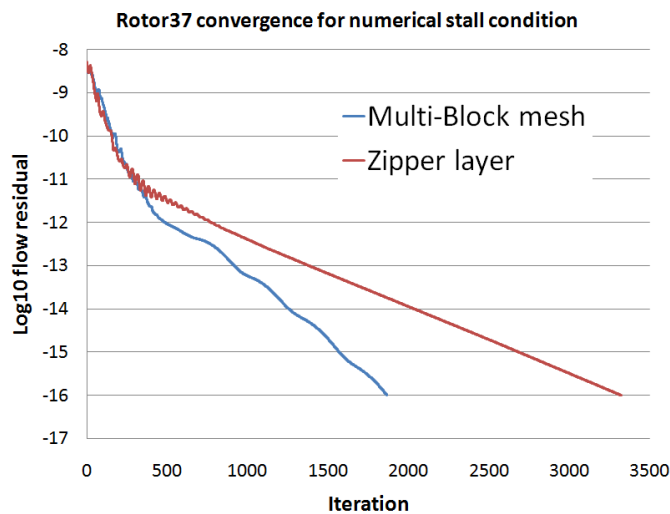


**Fig. 7** Convergence histories for the zipper layer mesh and structured MB mesh at stall

#### 4.0 METHOD OF GROOVE CASING TREATMENT OPTIMISATION

##### 4.1 Design Variables

Initial parametric tests were performed with an arbitrary six groove configuration and configurations based on the work of Huang *et al.* [11] and Choi *et al.* [13] and Beheshti *et al.* [10]. Therefore a six groove configuration was selected for the optimisation process; each groove could vary in height from 0-18% axial tip chord and the groove width from 6-10% axial tip chord. The first groove started from 0% axial tip and then allowed to vary depending on the groove width. The same groove width would be used for all grooves. This range would

encompass all possible uniform groove heights and widths determined from literature. By allowing the groove height to go to 0% axial tip chord, effectively removing the groove, this would add an extra dimension to the study as there are published results where [11] has no groove positioned above the blade tip LE and [13] which do have a groove above the blade tip LE. Hence by allowing each groove height to vary one should be able to determine a height sequence. This is logical as the strength of the tip vortex changes as it moves downstream, thus one should in theory require a change in groove height that will positively affect the flow field, as noted earlier a groove at the TE each was not significantly beneficial.

##### 4.2 Design of Experiment

A DoE technique has been selected that would give a good overall spread of points with a relatively small amount of simulations. Based on the initial parametric study the grooves starting aligned with the blade tip LE and up to 80% axial tip chord. Therefore seven parameters were used for the DoE, six grooves with independent height plus the groove width. The resulting groove parameters generated using the LPTau DoE [20]. An example of the different groove configurations generated from the LPTau DoE is shown in Fig. 8. With Kriging being used to build the RSM at least 70 groove configurations would have to be run. Approximation methods such as RSMs have found an increasing use in the optimisation of complex engineering systems [21]. Kriging is based on a Gaussian stochastic process method and provides a better approximation model than the traditional response surface methods based on first or second order polynomials. This is due to their abilities to interpolate sampled data and to model a function with multiple local extrema as the true surface for these complex models rarely adhere to a low polynomial shape. More details on the individual aspects of the design optimisation cycle such as the DoE and RSMs are given in [20]. The hyperparameter tuning strategy used was ARMOGA+SQP. This is a single genetic algorithm search (ARMOGA) followed by a gradient based 2<sup>nd</sup> order optimisation algorithm (SQP). The optimisation algorithm used to search the data space to determine an optimum point was the simulated annealing (S.A.) algorithm.

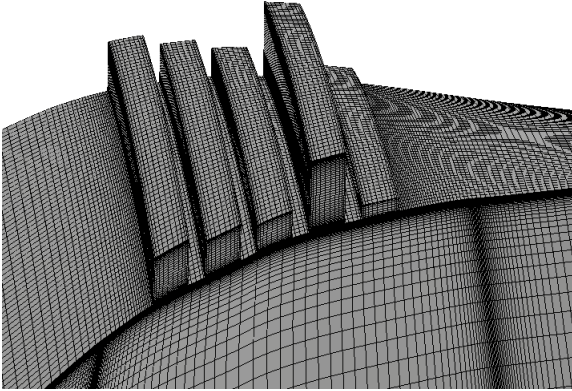


Fig. 8 Five groove configuration from LPtau DoE

### 4.3 Objective Function

The increase in stall margin was chosen to be the overall aim of improvement for the rotor. Reid and Moore [22] defined the stall margin as a comparison of stall to a reference value, in this instant the reference value used is the peak condition.

$$SM = \left[ \frac{PR_{stall}}{PR_{peak}} \times \frac{\dot{m}_{peak}}{\dot{m}_{stall}} - 1 \right] \times 100 \quad (4)$$

After testing a sample of configurations it was found that the peak efficiency and pressure ratio were not changing significantly compared to the base line model, which makes use of the zipper layer mesh as shown in Fig. 6. The main purpose of the groove casing treatment is to extend the operating range of the rotor whilst maintaining its overall efficiency. Therefore for a groove configuration to be considered it must first and foremost increase the operation range by stalling at a lower mass flow rate. Thus for a change in SM the factor that would give significant change is the stall mass flow rate, as the greater the change in mass flow should result in a greater change in SM, when compared to the base line model. Therefore the objective function used for optimisation process is the change in mass flow rate  $\Delta\dot{m}$ . The SM will be calculated only if a configuration first proves to be effective in extending the operating range. This therefore keeps the number of CFD simulations down to a minimum. With the possibility of multiple configurations being produced that increased the stall mass flow rate, the SM was also subject to the constraint that the peak efficiency did not deteriorate to better vet the groove configurations.

## 5.0 RESULTS AND DISCUSSION

### 5.1 Optimised Results

The validation of the zipper layer is given in Section 3.1 and compared to both the experimental data and the computational

CFD data using a MB structured mesh for Rotor 37. Thus, using the zipper layer meshing method for the groove casing treatment the DoE results for seventy two different configurations were used to construct the RSM. After searching for an optimum point the groove configuration was then made and tested computationally to find the near stall mass flow rate. A LOOCV was also calculated for each new configuration to assess the accuracy of the model. If the new configuration was found not to have provided the desired effect, it was still used to update the RSM model and a new search was performed to find another optimum point. The root square mean error (RSME) of the RSM was on average +/- 0.065Kg/s for all cases run. As one looks to extend the operating range of the rotor one actually aims to obtain a lower mass flow rate. This means that if the casing treatment configuration result produces the upper limit of the expected prediction the resultant mass flow rate and subsequent SM would not give an improvement. Similarly the opposite applies if the casing treatment configuration gives the lower limit then an improvement to the SM will be found. The whole optimisation cycle was performed using Rolls-Royce in-house software called SOPHY (SOFT-PADRAM-HYDRA) [3].

Before commencing with the optimisation process for the groove casing treatment for Rotor 37 a reference case was made. This case was made to set a bench mark for the optimiser to beat. The groove configuration of Huang et al. [11] had shown to be a good configuration. This configuration was therefore selected and subsequently altered by the author. It was concluded that the last groove did not play an important role in improving the SM, thus the number of grooves were reduced from 7 to 6. Thus a mesh with 6 grooves and depth (2mm) as specified in [11] was run, also based on other parametric models ran by the author the same mesh was made but this time the groove depth was reduced to 1mm. It transpired that the 1mm case gave the better SM. Hence this case was selected as the reference groove case. The result from the reference case was not added to the RSM, thus ensuring that a bias would not be included to the model.

In total ten updates to the RSM were performed. On several occasions the SM was shown to be an improvement when compared to the structured MB mesh with zipper layer mesh result. However it took till the tenth update in which the groove configuration also improved upon on the SM of the reference groove case. For the RSM and optimum search that finally produced the optimum groove configuration the optimiser, SOFT, had predicted a mass flow rate of 18.850Kg/s +/- 0.068Kg/s based on the LOOCV. The actual mass flow calculated by the CFD model was 18.797Kg/s, which is within the predicted error range. This is an improvement as previously without groove casing treatment the rotor stalled at a mass flow of 18.914Kg/s, see Fig 10. The numerical stall for the rotor without casing treatment differs from that of the experimental result, see Fig 6. Therefore for clarity the numerical mass flow rate of the rotor, without

casing treatment, is plotted in Fig 10 and is referred to as the RANS near stall. The reference groove configuration stalled at 18.795Kg/s, however, the SM is calculated based on the peak and stall condition, and as will be explained next the reference groove fared worse when it came to maintaining the peak efficiency. The final optimised groove configuration [23] is shown in Fig. 9. Details of the novel groove configuration where the depth size peak at mid chord are given in Table 1. The complete performance characteristics for the groove cases, with highlighted improvement, is shown in Fig. 10 with the resultant SM and efficiency results highlighted in Table 2. In Table 2 the structured MB mesh with zipper layer is referred to as the case with “no casing treatment”. As can be seen from Table 2 the optimised groove configuration not only has a better  $\Delta SM$  result than the reference groove case, 0.726% as compared to 0.7%, but also the peak efficiency is virtually unchanged when compared to a mesh with no casing treatment, -0.055% as compared to -0.742%. The SM has increased by 0.726% from the original value of 15.061% for the rotor with no casing treatment, this is an increase in the SM of nearly 4.8%. This therefore meets the required objective of finding an optimum groove configuration that can extend the operating range of Rotor 37 and yet maintain its original peak performance. The convergence history, from the CFD solver Hydra, for the optimised groove configuration at stall is given in Fig. 11. As previously commented on in section 3 it is vitally important that the back pressure used for the near stall margin does actually give a converged result, and that the mass flow rate is therefore stable. The next section will detail the change in flow physics that have occurred as a result of the introduction of optimised groove casing treatment.

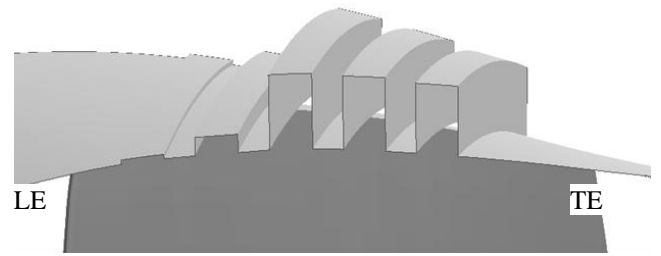


**Fig. 9** Optimised groove configuration based on optimum results from optimiser SOFT

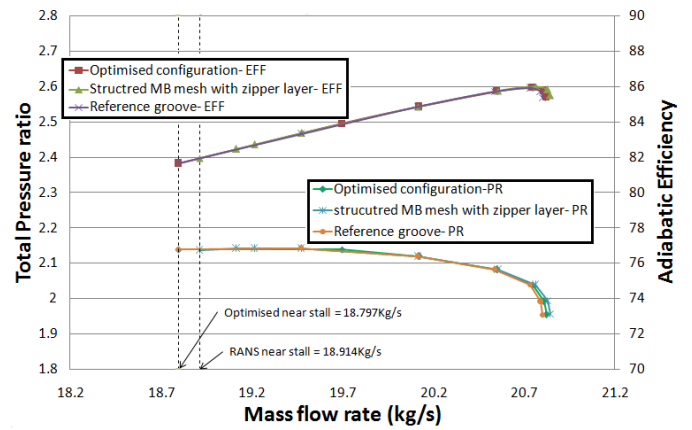


**Fig. 10** Comparison of CFD data for groove casing treatment for Rotor 37 when compared to mesh without groove casing treatment

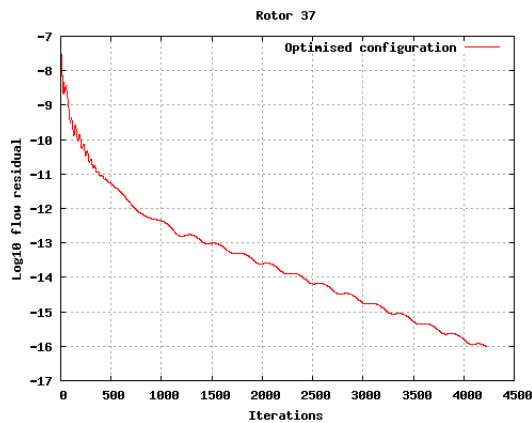
	SM(%)	$\Delta SM$ (%)	$\eta_{Peak}$ (%)	$\Delta \eta_{Peak}$ (%)
No casing treatment	15.061	–	85.831	–
Reference groove configuration	15.760	0.700	85.089	-0.742
Optimum groove configuration	15.787	0.726	85.776	-0.055

**Table 2** Comparison of stall margin and efficiency for differing groove casing treatment

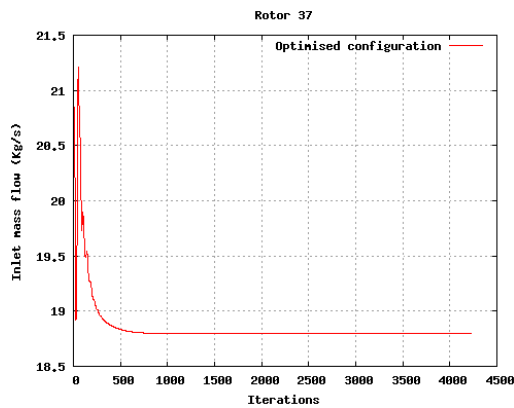
	Groove 1 depth (%AC)	Groove 2 depth (%AC)	Groove 3 depth (%AC)	Groove 4 depth (%AC)	Groove 5 depth (%AC)	Groove 6 depth (%AC)	Groove width (%AC)
Optimised grooves	0.0	1.1	4.3	17.5	17.0	16.1	8.3
Reference grooves	0.0	3.6	3.6	3.6	3.6	3.6	8

AC - Axial Chord

**Table 1** Groove parameters for both the optimised and reference casing treatment configurations



(a)



(b)

**Fig. 11** Convergence histories of Rotor 37 for (a) flow residual (b) inlet mass flow rate

## 5.2 Flow Physics of Groove Casing Treatment

With the optimised groove case showing improvement to the performance of Rotor 37 this section shall show how the flow has been changed by the presence of the grooves. The load on a blade can be categorised into three main regions, the high load region near the leading edge, a medium load region which lies between the high load region to just past the shock and finally the low load region near the trailing edge. The high load region is caused by the high relative incident angle of the casing boundary layer. Along with the pressure difference between the pressure and suction side a strong tip vortex is released that travels across the passage and towards the pressure side of the adjacent blade. The medium loaded region is where the shock has formed, and hence the load is a result of this. It is these two regions that eventually lead to the rotor stalling as the back pressure is increased. A low moving region of fluid in the mid passage of the rotor eventually blocks the passage enough that the fluid angle onto the blade

leading edges starts to increase. The increase in tip incident angle eventually leads the fluid to separate and stall therefore occurs.

Thus by aiding the flow in the passage, that is to re-energise it, one can improve the fluid flow. Therefore by considering the effect of the high/medium region one can design a suitable configuration that will be able to account for the difference in the flow field across the blade tip. Thus two key factors in determining the orientation and geometry of the grooves are:

1. A tip leakage vortex will always emanate from the blade tip leading edge, even if a casing groove is placed above it as there will always be a pressure difference resulting from the pressure and suction side. Therefore at best one will only be able to influence the direction of the tip leakage vortex. Hence the position of the first groove on the casing should be placed after the highly loaded blade tip region.

2. If a shock exists, its presences on the blade and its strength can be disrupted by re-energising the flow in the region local to the shock.

Applying these principles lead to the positioning of 6 grooves on the rotor. The first groove by the leading edge was found through optimisation to have zero height, therefore does not exist. The second groove which is just after the high load region (normally 0 – 10% axial chord) starts at 15% axial chord and can be seen in Fig. 12. Fig. 12 shows the static pressure distribution near the blade tip. The third groove position ends just at the start of the shock and as can be seen from Fig. 12 the presence of the grooves has altered the shock position. The fourth groove ends at the foot of the shock, the disruption to the shock can be seen in Fig. 13 which shows the relative Mach number near the blade tip, 99% span, at the stall condition of the rotor without and with circumferential groove casing treatment. The green region parallel to the blade pressure surface has expanded, indicating a faster flow speed around the tip. What is also obvious from Fig. 13 is that the grooves 4, 5 and 6 also contribute to increasing the fluid velocity in the passage by the periodic boundary. This increase in velocity of the fluid helps prevent the rotor from stalling by reducing the blockage in the passage. The spill forward region which indicates the incident angle of the fluid on to the blade tip has also been altered by the circumferential groove casing treatment for the better, see Fig. 14. Fig. 15. shows the tip leakage vortex path via the stream lines emanating from the blade tip surface, which seems to show little difference in the two TLVs.

If the grooves have been successful in altering the TLV the pressure ratio and efficiency of the rotor should increase, as the blockage should be slightly relieved and therefore the overall loss should decrease as the rotor has still not stalled. Fig. 16 shows the radial distribution of the mass averaged

profiles of the rotor for both total pressure ratio and adiabatic efficiency at station 4, this is a location 10.67cm downstream from the blade leading edge. Both groove configurations and the zipper layer mesh with no casing treatment are shown and all are at the same boundary condition, in this instance the back pressure at which the zipper layer mesh stalled. At this boundary condition the optimised groove mesh result indicates a slight increase in total pressure ratio and efficiency. This increase in efficiency should not be confused with the efficiency at the peak flow condition. At this point the efficiency did actually decrease slightly as indicated in Table 2.

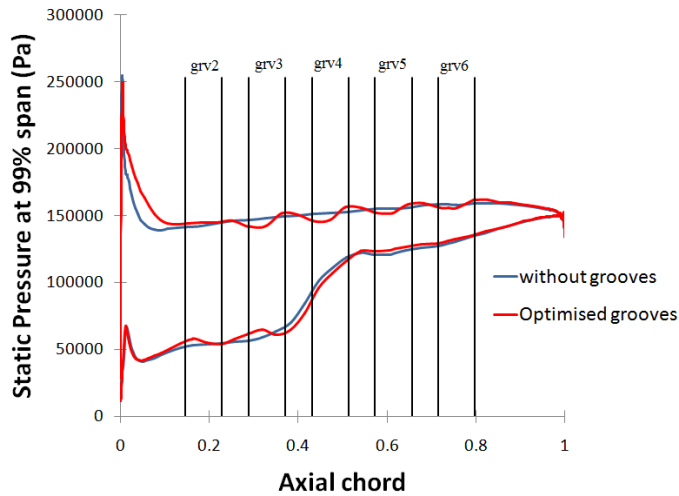


**Fig. 12** Pressure distribution on blade surface at 99% span at the stall point of the structured MB mesh with zipper layer with groove position indicated by black vertical lines.

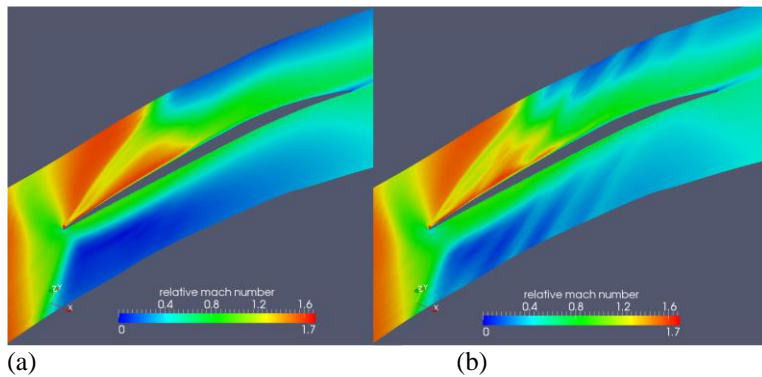


**Fig. 13** Relative Mach number contour near blade tip for the rotor (a) without casing treatment and (b) with casing treatment

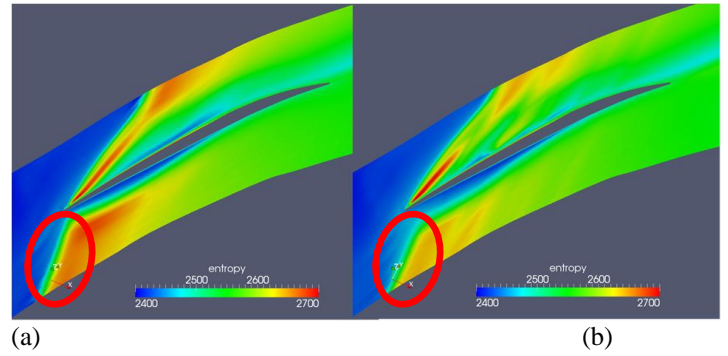


**Fig. 14** The spill forward region is indicated by the red circle for the rotor by means of entropy contours (a) without casing treatment and (b) with casing treatment

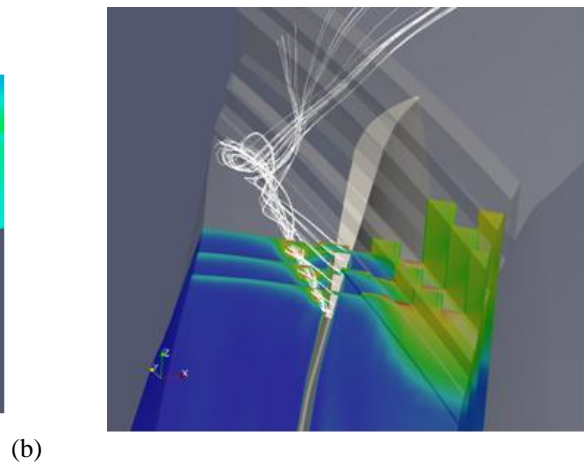
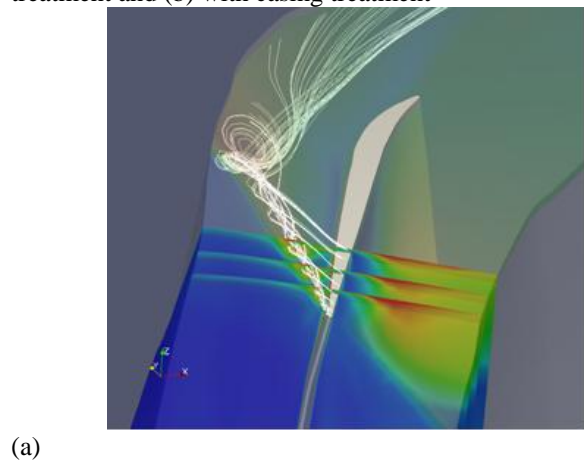


**Fig. 15** Tip leakage vortex path indicated via the stream lines emanating from the blade tip leading edge shown with entropy contours slices at varying axial position along the blade: (a) without grooves (b) with grooves

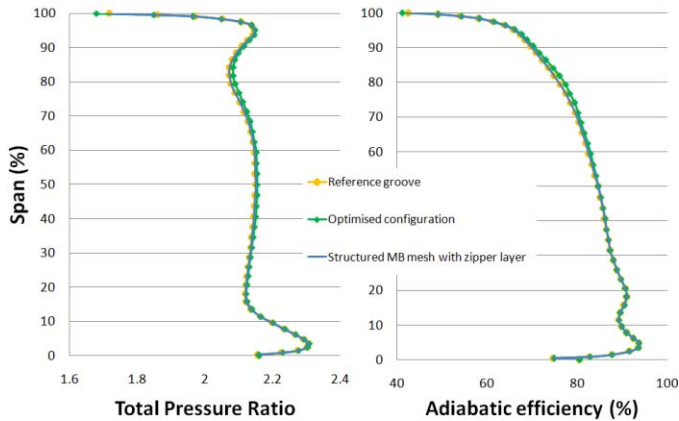


**Fig. 16** Mass averaged Rotor 37 profiles at stall point of structured MB mesh with zipper layer, at station 4, for (a) total pressure ratio (b) adiabatic efficiency

## 6.0 CONCLUSIONS

The paper has shown the optimisation of groove casing treatment making use of a novel mesh technique to link together two different topological structured meshes. The zipper layer method negates the need for interpolation and has been shown to be a valid and accurate mesh generation process. The object of this research is to determine an optimised groove configuration that would increase the operating range of the rotor while maintaining the rotors original efficiency. The optimisation process utilised a Kriging RSM as its surrogate model. A DoE was built based on the Sobol (LPtau) sequence and was used to construct the RSM. To search the data space to determine an optimum point the simulated annealing algorithm was employed. After retraining the model with continuous updates based on the CFD result of a given groove setup a configuration was finally determined that satisfied the objective of the research. The success of the optimisation process was based on not only surpassing the stall margin of a non-groove case, but also that of a configuration based on parametric studies. A stall margin improvement of 0.73% was achieved with virtually no loss in terms of peak efficiency. The casing groove played a vital role in that they relieved the flow blockage at what was the normal stall point of the rotor before groove casing treatment was applied.

## ACKNOWLEDGEMENTS

We would like to thank Dr. L. Lapworth of Rolls Royce plc. for his consultation regarding Hydra and the Rotor 37 test case, and Dr. C. Brooks of Southampton University for his advice regarding the Kriging optimisation process in SOFT. We would also acknowledge financial support from Roll Royce Plc. through the CFMS ICAST project and the permission by Rolls Royce Plc. to publish this work.

## REFERENCES

- [1] *Qin, N., Carnie, G., LeMoigne, A., Liu X., Shahpar, S.*, "Buffer Layer Method for Linking Two Non-Matching Multi-block Structured Grids", 47th AIAA Aerospace Sciences Meeting Including The New Horizons Forum and Aerospace Exposition, 5 - 8 January 2009, Orlando, Florida, AIAA-2009-1361
- [2] *Shahpar, S., Qin, N., Wang, Y. and Carnie, G.* "A Method of Connecting Meshes", GB Patent number 1101810.8
- [3] *Shahpar, S.*, "SOPHY: An integrated CFD based Automatic Design Optimisation System", ISABE-2005-1086
- [4] *Osborn, W. M., Lewis, Jr., G. W., and Heidelberg, L. J.*, "Effect of several porous casing treatments on stall limit and on overall performance of an axial-flow compressor rotor", NASA TN D-6537, 1971
- [5] *Suder, K. L., Celestina, M. L.*, "Experimental and computational investigation of the tip clearance flow in a transonic axial compressor rotor", ASME J. Turbomachinery., 118 pp. 218-229, 1996.
- [6] *Adamczyk, J. J., Celestina, M. L., and Greitzer, E. M.*, "The Role of Tip Clearance in High-Speed Fan Stall", ASME Journal of Turbomachinery, Vol. 115, pp. 22-38, 1993.
- [7] *Thompson, D. W., King, P. I., and Rabe, D. C.*, "Experimental investigation of stepped tip gap effects on the performance of a transonic axial flow compressor rotor", ASME J. Turbomachinery, Vol. 120 pp. 477-486, 1998.
- [8] *Shabbir, A., and Adamczyk, J. J.*, "Flow mechanism for stall margin improvement due to circumferential casing grooves on axial compressors", ASME Journal of Turbomachinery, Vol. 127, pp. 708-717, 2005.
- [9] *Ito, Y., Watanabe, T., and Himeno, T.*, "Effects of Endwall Contouring on Flow Instability of Transonic Compressor", International Journal of Gas Turbine, Propulsion and Power Systems, Vol. 2, No 1, pp. 24-29, 2008.
- [10] *Beheshti, B. H., Teixeira, J. A., Ghorbanian, K., and Farhanieh, B.*, "Parametric Study of Tip Clearance – Casing Treatment on Performance and Stability of a Transonic Axial Compressor", ASME Journal of Turbomachinery, Vol. 126, pp. 527-535, 2004.
- [11] *Huang, X., Chen, H., Shi, K., and Fu, S.*, "CFD investigation on circumferential grooves casing treatment of a transonic compressor", ISABE-2009-1185.
- [12] *Chen, H., Huang, X., and Fu, S.*, "CFD investigation on stall mechanisms and casing treatment of a transonic compressor", 42<sup>nd</sup> AIAA/ASME/SAE/ASEE Joint Propulsion Conference & Exhibit, 2006, AIAA 2006-4799
- [13] *Choi, K-J., Kim, J-H., Kim, K-Y.*, "Design optimization of circumferential casing grooves for a transonic axial compressor to enhance stall margin", Proceedings of ASME Turbo Expo 2010: Power for Land, Sea and Air GT2010, GT2010-445;8
- [14] *Sobol, I. M.*, "On the systematic search in a hypercube", SIAM Journal of Numerical Analysis, Vol. 16, pp-790-793, 1979.

- [15] *Forrester, A.I.J, Sobester, A., Keane, A.J.*, "Engineering design via surrogate modelling: a practical guide", Chichester: Wiley; 2008
- [16] *Dunham, J.*, "CFD Validation for Propulsion System Component", AGARD-AR-355, 1998
- [17] *Shahpar, S., and Lapworth, L.*, "PADRAM: Parametric Design and Rapid Meshing System for Turbomachinery Optimisation", ASME GT2003-38698, Atlanta, Georgia, 2003
- [18] *Lapworth, L.*, "Hydra-CFD: a framework of collaborative CFD development", International Conference on Scientific and Engineering Computation, Singapore, July 2004.
- [19] *Sethian J A.* Fast marching method. SIAM review, vol. 41, No. 2, pp199-235,1999.
- [20] *Shahpar, S.*, "Design of Experiments, Screening and Response Surface Modelling to Minimise the Design Cycle Time", *invited lecture at VKI, Belgium, 2005*
- [21] *Shahpar, S.*, "A Comparative Study of Optimisation Methods for Aerodynamic Design of Turbomachinery Blades", ASME Paper 2000-GT-523, 2000.
- [22] *Reid, L., and Moore, R. D.*, "Performance of Single-Stage Axial-Flow Transonic Compressor With Rotor and stator Aspect Ratios of 1.19 and 1.26, Respectively, and With Design Pressure Ratio of 1.82", NASA TP-1338, 1978.
- [23] *Shahpar, S., Qin, N., Carnie, G. and Wang, Y.* "A Turbomachine Comprising an Annular Casing and a Bladed Rotor", GB Patent number 1101811.6